

THE STRUCTURE AND EVOLUTION OF THORNE-ŻYTKOW OBJECTS

R. C. CANNON¹ AND P. P. EGGLETON¹

Institute for Theoretical Physics, University of California at Santa Barbara, CA 93106

AND

A. N. ŻYTKOW AND P. PODSIADŁOWSKI

Institute of Astronomy, Madingley Road, Cambridge CB3 0HA, UK

Received 1991 April 1; accepted 1991 August 2

ABSTRACT

We construct models of spherically symmetric stars in which a central neutron star core is accreting material from an envelope (Thorne-Żytkow objects or TŻOs). Core masses are allowed to grow by accretion from ~ 0.5 to $2.0 M_{\odot}$, and envelope masses range from ~ 0 to $30 M_{\odot}$. We find models populating the entire range of both parameters, and a limited range of parameter space in which two distinct types of model can coexist, one where gravitational energy and one where nuclear energy is the dominant source of energy.

Subject headings: stars: interiors — stars: neutron

1. INTRODUCTION

There are at least two circumstances in which it can be anticipated that a star will be formed which has a neutron star or black hole core at the center of a normal stellar envelope: such a star will be referred to as a “Thorne-Żytkow object” or TŻO (Thorne & Żytkow 1975, 1977; hereafter collectively TŻ). The circumstances are as follows:

1. In a globular cluster, a direct or near-direct collision between a neutron star and a normal star (dwarf or giant) may result in the capture and coalescence of the two objects into a single object (Ruffert & Müller 1990).

2. In a massive X-ray binary (MXRB), evolution of the massive normal star may cause it to engulf the neutron star companion, leading to a common envelope, spiral-in, and ultimately complete coalescence.

The former process may lead to TŻOs of ~ 2 – $3 M_{\odot}$, while the latter might lead to TŻOs of considerably greater mass. In this paper, we examine simple models of TŻOs over a considerable range of both core mass (0.5 – $2 M_{\odot}$) and envelope mass (~ 0 – $30 M_{\odot}$). Unlike the original investigation by TŻ, we model the entire star instead of just the envelope down to the radius and mass of an assumed neutron core; we therefore do not have to make the assumption of steady state mass inflow, although our models do show just such a steady state inflow in practice. We do however make some different simplifications in the present investigation, although with the intention of removing them in later investigation. In particular, for the present we neglect all nuclear reactions except the burning of hydrogen to helium, and we do not yet attempt the refinements of very high temperature hydrogen burning, such as the interruption of CNO or NeNa cycling by β -decays which are slow compared with proton capture. In effect we assume that hydrogen burns to helium by the usual CNO cycle, and that the helium then metamorphoses directly (by means of an artifice) into neutrons at an approximately high density. Since all the reactions between helium burning and neutronization involve only the release of $\sim 15\%$ as much energy as hydrogen burning, we feel that this approximation can be justified in some circumstances.

Before discussing our computational procedure, in § 2, we consider in a little more detail the second possibility above. Although it may seem likely, even inevitable, that MXRBs will evolve into a common envelope (CE) configuration, because Roche lobe overflow (RLOF) will transfer matter at such a considerably super-Eddington rate that the compact component will be unable to accept most of it, there is at least one reason for supposing that the end result will not be coalescence into a TŻO; and there is also at least one reason for supposing that the system will respond to rapid mass transfer by some mechanism that avoids a CE phase. First, it is rather likely that close double neutron star binaries such as 1913+16 (Hulse & Taylor 1975) are formed by CE evolution without coalescence. The kind of scenario (Flannery & van den Heuvel 1975) invoked to explain 1913+16 requires that the CE be formed when the massive normal star has evolved to a yellow or red supergiant with central helium burning, or perhaps a little beyond. It is then assumed that the CE is ejected after considerable spiral-in, but before complete coalescence would occur, leaving a close binary with a period of 3 or 4 hr containing a helium-burning star of $\gtrsim 3 M_{\odot}$ along with the original neutron star. This companion can then become a supernova and leave a neutron star remnant without disrupting the system, although the explosion should generate the substantial eccentricity seen in 1913+16. It is hard to see what other evolutionary mechanism might produce such a double neutron star binary, and so it is hard to escape the conclusion that at least *some* MXRBs avoid coalescence despite undergoing CE evolution with spiraling-in.

The second reservation is that the binary V1343 Aql (SS 433; Margon 1984; Crampton & Hutchings 1981) is presumably an example of rapid mass transfer from an evolved OB star to a neutron star or black hole; but instead of forming a CE, the binary seems to be evolving in a quite different way. In particular, the material falling into the Roche lobe of the compact star does not appear to be filling up that lobe to form a CE, but instead some or all of it is being squirted into space in bipolar relativistic jets. Conceivably the whole envelope will be ejected, perhaps partly by jets and partly by a Wolf-Rayet-like wind from the hot star, without the orbital period being reduced by two orders of magnitude.

Our counter to the first point is that we expect complete

¹ On leave from Institute of Astronomy, Cambridge.

coalescence to occur only if the orbital period of the initial MXRB is quite small, perhaps as small as 1–3 days; so that the primary fills its Roche lobe before, or very shortly after, central hydrogen is exhausted. Examples (Joss & Rappaport 1984) of such MXRBs are V779 Cen (Cen X-3: NS + O6.5 II; 2^d1), LMC X-3 (NS/BH + B3 V; 1^d7) and LMC X-4 (NS + O7 III; 1^d4). In these systems the OB star's core at RLOF will be only a little more compact than on the ZAMS. By contrast, the OB star in the longer period MXRB BP Cru (NS + B1.5 I; 41^d) will probably already have a relatively compact helium-burning core, and even more so when it arrives at RLOF. The latter kind of system may emerge from a CE phase as a progenitor of a double neutron star binary, while the former is more likely, we believe, to proceed to complete coalescence and a massive TZO.

Our counter to the SS 433 analogy is mainly that because this system is apparently unique it is difficult to argue that it is “typical” of some normal evolutionary stage of an MXRB. It may represent a short-lived ($\sim 10^3$ – 10^4 yr) stage as mass transfer accelerates from stellar wind accretion to RLOF. Perhaps the OB star has a wind which is comparable in strength to a WR star, but which is not yet as copious a flow as expected from RLOF. We note that one model of SS 433 (Fabian et al. 1986) attributes the jets to a mechanism in which the presumed OB companion is merely a spectator rather than a participant.

The lifetimes of TZOs are determined by how rapidly they exhaust their envelopes, due to accretion onto the core and due to mass loss from the surface (where the latter is generally the dominant process). After TZOs have lost their envelopes, they will leave a single neutron star or black hole remnant. If the remnant is a rapidly rotating neutron star, it may appear as a millisecond pulsar (with a spin period $\lesssim 100$ ms). Indeed, in any binary formation scenario, we expect that, immediately after the spiral-in phase, the material just above the neutron core, which will subsequently be accreted by the neutron core, has sufficient angular momentum to spin up the neutron star to millisecond periods. Whether this process provides a viable mechanism to produce single millisecond pulsars depends on how much mass is accreted (which in turn depends on the lifetime of the TZO phase) and how angular momentum is redistributed within the envelope after the spiral-in phase.

The early work on stars with neutron cores was discussed in TŻ and Eich, Zimmerman, & Thorne (1989). TŻ discussed two classes of models: *giants* for which 97% of their energy comes from accretion of envelope onto the core, and *supergiants* for which about 95% of the energy comes from nuclear burning at the base of the convective envelope. Zimmerman (1979), summarized in Eich et al. (1989), attempted unsuccessfully to construct improved models of *supergiants* taking into account some aspects of nonequilibrium nucleosynthesis in the “burning zone.” He could not find self-consistent models of *supergiants* since in his approximation nuclear reactions produced no more than ~ 0.04 of the required luminosity. Recently, Biehle (1991) has shown that viable models of *supergiants* can be constructed if the rp process (rapid, direct addition of protons onto nuclei) is taken into account since then sufficient energy can be generated.

The observational detection of TZOs will be difficult, since to a distant observer, the extreme conditions of the central parts of these objects are hidden by the huge red giant envelope. TŻ suggested that chemical anomalies in the atmospheres of *supergiants* may form a possible observational signature of such stars. Biehle (1991) has explored a possible

observational signature of his *supergiant* models and suggested investigating abundances of ⁸⁴Sr in cool stars. If TZOs form in globular clusters (as discussed above), they may be easier to detect, since they would probably outshine all other stars in the cluster. However, there is a danger that they could be mistaken for foreground field stars, proving the cluster membership of any TZO candidates would be essential. Phinney & Kulkarni (1991) review the tidal capture processes in globular clusters which involve single neutron stars. The possible outcomes of such events may include the formation of TZOs as well as low-mass X-ray binaries. We expect that the number of TZOs should scale like the number of low-mass X-ray binaries times the ratio of their respective lifetimes. While the lifetimes of both types of systems are poorly known, we estimate that there should be at most a few observable TZOs in the whole globular cluster system (this assumes that TZOs with low-mass envelopes are dynamically stable, which need not be the case).

2. COMPUTATIONAL METHOD

Using a modified version of the stellar evolution code developed by Eggleton (1971, 1972, with substantial later modifications), we have constructed a range of models with core masses from 0.4 to 2.0 M_{\odot} , and envelope masses from ~ 0 to 30 M_{\odot} . For low envelope masses or high core masses, the dominant energy source is accretion, and all nuclear reactions take place below the convection zone and may be adequately modeled by conventional methods. For envelope masses $M_{\text{env}} > 7 M_{\text{core}}$, significant burning takes place in the first few hundred meters of the convection zone, and this becomes potentially the most important source of energy. Here we make a simple approximation to the energy supply under such circumstances: the detailed modeling of reaction networks in such stars is to be the subject of a later paper in this series.

The relativistic equations of stellar structure are used throughout, in the formalism by Thorne (1977) which makes easy contact with the standard Newtonian scheme. Two equations are required, one for the gravitational potential and one for the gravitational mass, in addition to the normal seven (five first-order equations for the structure variables m , r , L , P , T ; one second-order equation for the hydrogen abundance and one “eigenvalue equation” for the mesh spacing constant C defined below). The former single-mass variable is now used to represent the rest mass, i.e., the baryon number \times rest mass of a hydrogen atom in its ground state.

We model the core as an integral part of the star, instead of imposing an inner boundary condition at the edge of the neutron core. We adopt a phenomenological general relativistic equation of state from Cooperstein (1988): case (2.5a) which has an Oppenheimer-Volkoff (OV) mass limit (Oppenheimer & Volkoff 1939) of 2 M_{\odot} for the effective mass, or 2.32 M_{\odot} for the rest mass. The radius–effective mass relation is plotted in Figure 1. A device is used to connect the core with the envelope at $\rho > 10^6$ g cm⁻³ in the region where, physically, inverse beta decay takes place. We alter the equation of state (Eggleton, Faulkner, & Flannery 1973) so that as the electrons become increasingly degenerate, their notional mass varies in the following way:

$$m'_e = \begin{cases} m_e, & \text{if } \psi < 0 \\ e^{\psi} m_e, & \text{if } 1 < e^{\psi} < k \\ km_e, & \text{if } e^{\psi} > k \end{cases} \quad (1)$$

where ψ is the electron degeneracy parameter. This gives the

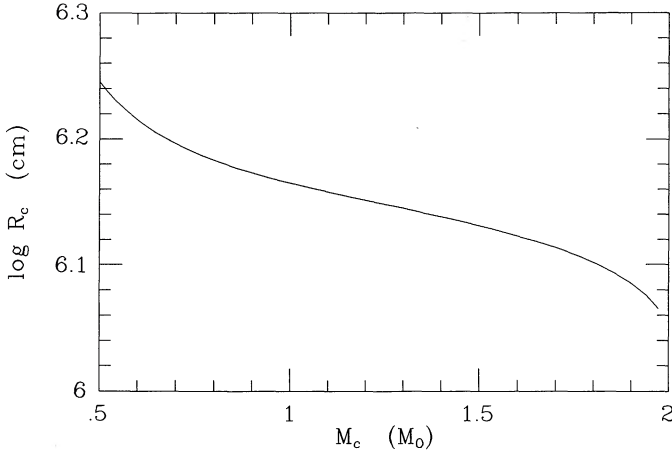


FIG. 1.—Core radius-mass relation: BCK equation of state case (2.5a) (Cooperstein 1988).

conventional Fermi-Dirac electron equation of state for $k = 1$ or $\psi < 0$; and beyond the upper limit on ψ it gives (in the case $k = m_n/m_e$) the Oppenheimer-Volkov (1939) equation of state for degenerate neutron material, which is then smoothly joined to the core equation of state. As this artificial region is very narrow and (TŽ) essentially decoupled, except gravitationally, from the rest of the star, we believe the numerical simplicity is justified.

Beginning with a conventional (i.e., $k = 1$) $1 M_\odot$ star which has developed a hydrogen-depleted core of about $0.2 M_\odot$, a TŽO model is produced by gradually increasing k at a constant logarithmic rate from 1 to 1836 ($= m_n/m_e$). We also found it necessary to eliminate energy release through hydrogen burning at the early stages of the ensuing core contraction, gradually reintroducing it later.

Burning at the base of the convection zone is modeled by calculating a convective inflow velocity for mixing down material from further out into the first few hundred meters above the knee. Above this we impose a fixed composition throughout: we are interested in the structure of stars formed with a core already in the upper half of the range we consider so do not wish to record the envelope composition changes that would have occurred during evolution from a model with a much less massive core. For all but the type C (§ 3) models with the most massive cores, this is equivalent to the usual “perfect mixing” approximation for convective regions.

The code uses a non-Lagrangian mesh with a fixed number (200) of points which are distributed, during the same Newton-Raphson iteration as the structure equations themselves, at equal intervals of a carefully chosen function Q . Schematically, Q is of the form $Q = m/m_\odot - \log P$. In the central core, where the pressure P is slowly varying, this means the code chooses approximately equal intervals of m . In the surface layers, where m is nearly constant, the code is obliged to choose nearly equal intervals of $\log P$. The mesh spacing is then given by

$$\Delta m_{k+1/2} \equiv m_{k+1} - m_k = (C/Q')_{k+1/2}, \quad (2)$$

where

$$Q' = \frac{dQ}{dm} = \frac{1}{m_\odot} + \frac{Gm}{4\pi r^4 P}. \quad (3)$$

C is a constant throughout the star, but may vary with time: an eigenvalue equation for C is solved simultaneously with the

structure and composition equations. The fact that Q' always has the same sign throughout the star, and hence that Q is monotonic, is of course important for constructing a viable mesh.

However, such a mesh distribution turns out to be inadequate for following the details of the release of gravitational energy in a TŽO because the release takes place in a very narrow region (typically a few meters, depending on the core mass) over which both the total pressure, almost entirely radiation pressure, and the mass hardly vary. However, this is exactly where, for infalling matter, gas pressure starts to be an important contributor to the total pressure, so we add a term in $\log P_g$ to Q ; more precisely, we add $\max(0, -d \log P_g/dm)$ to dQ/dm to ensure that Q is monotonic.

This yields a sufficiently fine mesh out as far as the base of the convection zone (hereafter “knee” in the notation of TŽ), but there the gas pressure scale height changes from \sim meters to \sim kilometers in the space of a few meters. This gives rise to a drastic near-discontinuity in Δm and leads to a breakdown of the difference approximations. Evaluating the mean in equation (2) as

$$\left(\frac{C}{Q'}\right)_{k+1/2} = \frac{1}{2} C \left[\frac{1}{(Q')_k} + \frac{1}{(Q')_{k+1}} \right], \quad (4)$$

corresponds to taking $\Delta m = \frac{1}{2}(\Delta m_k + \Delta m_{k+1})$ where $\Delta m_{k+1} = C/(Q')_{k+1}$. Suppose that, for some m_0 , Q' falls faster than $(m - m_0)^{-1}$ as happens at the knee in our models; then $Q'/\Delta m_{k+1}$ falls as m increases, there is no solution for Δm , and the next mesh point is driven out to where Q' levels out. This may correspond to a change by several orders of magnitude in dQ/dm . The immediate problem may be overcome by taking a harmonic instead of an arithmetic mean for equation (4), but even then situations arise in which the change in mesh spacing becomes unacceptably abrupt.

Instead, we adopt a more general approach, replacing the locally evaluated quantity δm_k defined as

$$\delta m_k \equiv (C/Q')_k, \quad (5)$$

by a further variable, $\delta^* m_k$, intended to follow δm_k as closely as is consistent with the constraints that $\delta^* m_k$ be a differentiable function of Q'_k and Q'_{k-1} and that $\delta^* m_{k+1}/\delta^* m_k < e^{1/\alpha}$ for some suitably chosen constant α . Defining

$$\beta = \frac{\delta m_{k+1}}{\delta^* m_k}, \quad (6)$$

and

$$\beta^* = \begin{cases} \beta & (\beta \leq 1) \\ \exp \frac{1}{\alpha} \left(\frac{\beta^{2\alpha} - 1}{\beta^{2\alpha} + 1} \right) & (\beta > 1), \end{cases} \quad (7)$$

then this may be effected by requiring

$$\delta^* m_{k+1} - \beta^* \delta^* m_k = 0. \quad (8)$$

The boundary condition $\delta^* m_1 = \delta m_1$ is imposed at the center. The mass increment is given by $\Delta m_{k+1/2} = \frac{1}{2}(\delta^* m_k + \delta^* m_{k+1})$. The choice $\alpha = 2$ has proved successful in our work so far, corresponding to a maximum increase in $\Delta m_{k+1/2}$ of about 1.7 between successive mesh points.

Note that $\delta^* m$ still falls as rapidly as δm , between the center and the energy-producing shell, so as to achieve the same minimum spacing as before, because of the boundary condition

imposed at the center. This fall is drastic, by up to 18 orders of magnitude in ~ 80 steps but is handled quite easily by the original mesh-spacing algorithm because δm decreases smoothly: in practice $\delta^*m_{k+1}/\delta^*m_k$ rarely falls below $e^{-1/2}$. It is only the increase beyond the shell, where δm leaps by several orders of magnitude in the space of a few steps, which is restricted.

Perhaps it is worth stressing the importance of a flexible mesh for these calculations. In a typical model, at the knee $\Delta m_{k+1/2} < 10^{-18} M_\odot$, while the mass accretion rate is $\sim 10^{-8} M_\odot \text{ yr}^{-1}$. With a Lagrangian mesh, the knee would have to move through many mesh points every second. On an Eulerian mesh the problem is less severe, but even then, the contraction of the accreting core amounts to at least $10^{-3} \text{ cm yr}^{-1}$, which may correspond to several mesh points in 10^4 yr . With a mesh tied to the structure through $\log P$ and $\log P_g$, we are comfortably able to take timesteps in excess of 10^5 yr for evolution at constant total mass.

Having generated an initial TZO model with a low-mass core, further models are generated by adding or removing mass at the photosphere, or simply by allowing the core to accrete as it runs its evolutionary course. The non-Lagrangian character of the mesh makes it particularly easy to change the total mass of the star it is only necessary to replace the boundary condition $m = \text{given}$ by, for example, $\dot{m} = \text{given}$, where \dot{m} is the rate of change of the total mass of the star.

3. RESULTS

Figure 2 shows the tracks taken by some of our models in the core mass (M_c) versus total mass (M_t) plane. Here (and throughout) we use the effective gravitational mass rather than the "rest mass." There is a boundary at low total mass $M_c = M_t$; the upper limit on the core mass comes from the OV limit of our equation of state, $M_c = 2.0 M_\odot$. Figure 3 shows evolutionary tracks on the H-R diagram for models $M_t = \text{constant}$.

With the exception of a small region $12 \lesssim M_t/M_\odot \lesssim 16$, $M_c \gtrsim 1.7 M_\odot$ we find a smooth variation of properties across

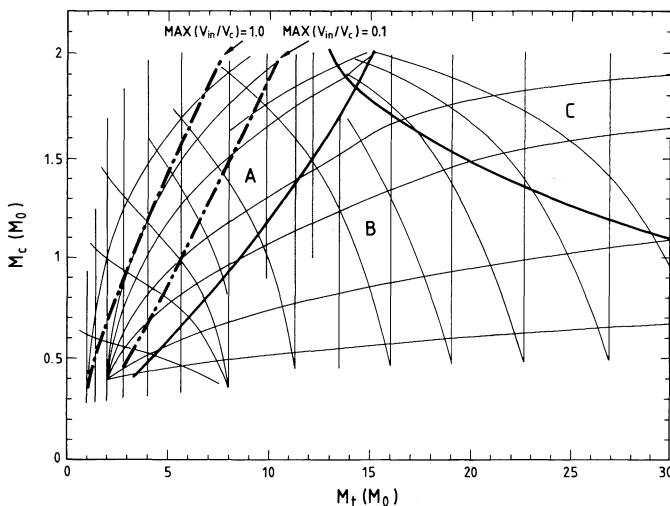


FIG. 2.—Tracks taken by some of our models while adding or removing mass at the photosphere, or keeping the total mass constant. The direction of evolution is toward higher core masses. Regions A, B, and C correspond to the structural classification in the text. Models lying above the line $\max(v_{\text{in}}/v_{\text{conv}}) = 1$ have inflow velocities somewhere exceeding the local convective velocity and must therefore be considered unphysical.

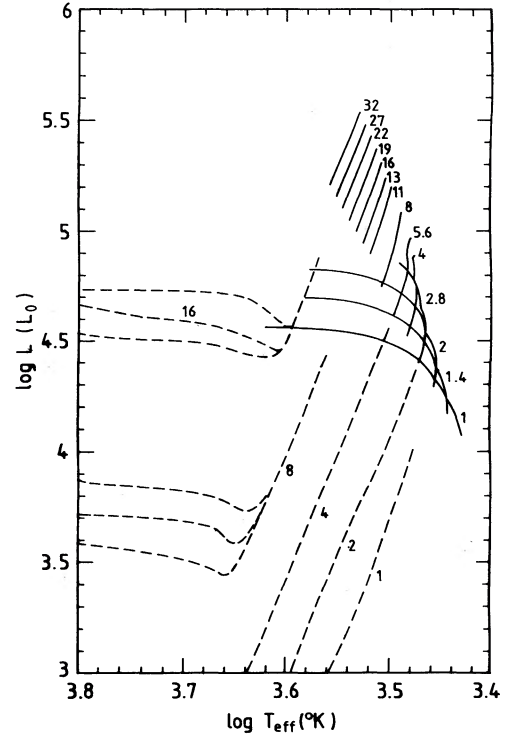


FIG. 3.—Tracks in the H-R diagram for models of different envelope mass evolving at constant total mass. Evolution is toward increasing luminosity in all cases.

the plane. In contrast to TŻ, we find no area without any solutions. Possible reasons for this discrepancy are considered at the end of this section. In several cases the same point has been reached by two or sometimes three different routes. We have examined all the cases where three tracks meet or nearly meet and, with the exception of models in the small region described above, find the different models indistinguishable. The variation of fundamental variables between models with the same (M_t , M_c) but different earlier histories is, at a given meshpoint, typically less than the difference associated with a change in core mass of $0.01 M_\odot$.

In all our models there is a deep convective envelope reaching down to within a few hundred meters of the core. At the base of the envelope, the "knee" is a very steep gas pressure gradient, with a scale height of a few meters or less, where infalling matter gives up its gravitational energy. The accretion rate is indirectly related to conditions at the knee through the force balance equation,

$$L_{\text{knee}} = L_r^{\text{crit}} \equiv 4\pi c G M_r \kappa^{-1}, \quad (10)$$

because the dominant contribution to L_{knee} is L_{grav} , the accretion luminosity, given by

$$L_{\text{grav}} = \frac{G M_c \dot{M}}{R_c}, \quad (11)$$

where for clarity we have omitted the relativistic correction factors used in the code.

Three broad classes of structures may be distinguished according to the relative contributions of nuclear reactions and accretion to the total luminosity, inhabiting approximately the regions A, B, and C shown in Figure 2.

(A).—The hydrogen burning shell is below the knee, so $L_{\text{nuc}} \approx 0.007Mc^2$ and there is no source of energy above the knee:

$$\frac{L_{\text{nuc}}}{L_{\text{grav}}} = 0.007 \left(\frac{GM_c}{Rc^2} \right)^{-1} \lesssim 0.08. \quad (12)$$

(B).—Some hydrogen burning takes place in the convection zone, but electron-positron pairs are unimportant everywhere:

$$0.08 \lesssim \frac{L_{\text{nuc}}}{L_{\text{grav}}} \lesssim 1. \quad (13)$$

(C).—Hydrogen burns in the convection zone and pairs dominate the opacity at the knee.

This increase κ in equation (10), reducing L_r^{crit} and hence L_{grav} and cutting down the accretion rate. Nuclear burning provides the shortfall in luminosity giving

$$1 \lesssim \frac{L_{\text{nuc}}}{L_{\text{grav}}} \lesssim 10. \quad (14)$$

Note that, because convection is able to feed fuel to the burning region from the large (in our models virtually inexhaustible) reservoir of the envelope, the nuclear luminosity is no longer limited, as in region A, to a constant and rather small steady state fraction of the gravitational luminosity.

Our models in region A with $1 M_{\odot}$ cores are in excellent agreement with those computed by TŻ and classified as giant type solutions. However, as shown in Figure 4, we find a rapid increase of the maximum inflow velocity as the core mass increases, to the extent that, taking for example a model of total mass $4 M_{\odot}$, when the core exceeds $1.4 M_{\odot}$, the maximum of the calculated inflow velocity exceeds the convective velocity though both are still well below the sound speed. Clearly the assumption of slow inflow in hydrostatic equilibrium must break down some way before this situation is reached. The contours in the M_c - M_t plane for which $\max(v_{\text{in}}/v_{\text{conv}}) = 0.1$ and 1 are shown in Figure 2.

TŻ find no structures similar to our case B, but instead a region with no solutions between about 9.5 and $11 M_{\odot}$ for a $1 M_{\odot}$ core and then “supergiant type” solutions, similar to our

case C with respect to the role of pair creation, at higher envelope masses. The evolutionary variation in luminosity and accretion rate for some typical models is shown in Figure 5.

For all our models except those above the $\max(v_{\text{in}}/v_{\text{conv}}) = 0.1$ line of Figure 2, the infall velocity at each point is smaller, by at least a factor of 10, than the convective velocity calculated from the standard mixing-length theory, which in turn is typically less than a hundredth of the sound speed: Figure 4 shows a range of velocity profiles. Under these conditions, the errors involved in the assumption of hydrostatic equilibrium, and the neglect of advective terms in our calculation of the radiation force on the fluid from the local flux instead of the flux in a frame comoving with the fluid (Miller 1990) are negligible.

Figure 5 shows a downturn in accretion rate for models of $\sim 16 M_{\odot}$ and above (evolving without mass loss) as they move from region B to region C. The temperature-density profile (Fig. 6a) varies smoothly meanwhile. The strong temperature dependence of pair creation,

$$\frac{n_+}{n_e} \propto \frac{\mu_e}{\rho} T^{3/2} \exp\left(-\frac{m_e c^2}{kT}\right), \quad (15)$$

where n_+ is the number density of positrons and n_e that of ionization electrons, is responsible via the opacity (Fig. 6b). For comparison, we also show the profile of the 12 and $5 M_{\odot}$ models calculated by TŻ (types A and C, respectively) and, in Figures 7a and 7b, the profiles of an $11 M_{\odot}$ type A model. In the TŻ supergiant, the knee is still sharp, with $n_+/n_e > 20$ owing to their assumption of perfect mixing and hence constant composition and high nuclear energy generation rates right down to the base of the convection zone. In the present calculations, under these extreme circumstances hydrogen is exhausted in a shallow region of a few hundred meters or so above the base of the convection zone, decreasing the temperature gradient, flattening the pair creation peak to $n_+ < 8n_e$, and thereby softening the knee. It should be noted that convection must be *very* efficient in mixing down material to be burned for the type C structure to be possible even supposing the reactions go to completion immediately. The maximum rate of supply of material to be burned in $\dot{m} = 4\pi r_{\text{knee}}^2 \rho v_{\text{conv}} <$

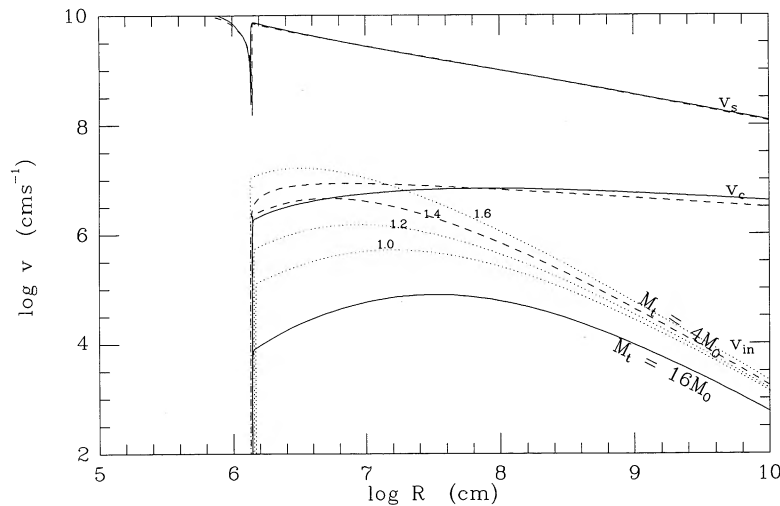


FIG. 4.—The sound speed v_s , convective velocity v_c , and velocity of inflow v_{in} , for models of type A ($4 M_{\odot}$, dashed line) and type C ($16 M_{\odot}$, solid line), each for a $1.4 M_{\odot}$ core. Also shown (dotted) are the v_{in} profiles for the type A model with core masses 1.0 , 1.2 , and $1.6 M_{\odot}$.

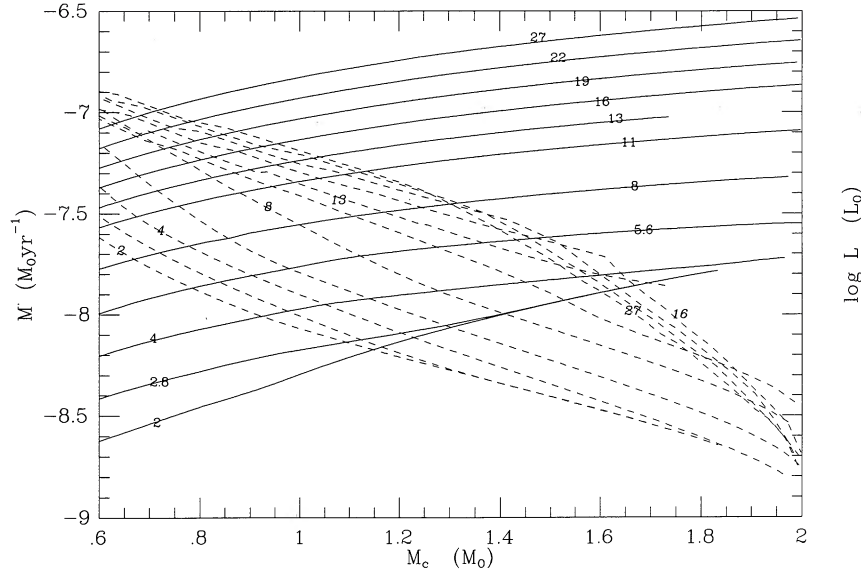


FIG. 5.—Accretion rate (dashed line) and luminosity (solid lines) as a function of core mass for models of constant total mass from 2 to $27 M_{\odot}$.

10^{20} g s^{-1} which can supply $\sim 0.007mc^2 < 7 \times 10^{38} \text{ ergs s}^{-1}$, i.e., at most $2 \times 10^5 L_{\odot}$, which is barely larger than the luminosity required to support the envelope.

In the small area of overlap between regions A and C, we find solutions characteristic of both classes. Two such models of $15 M_{\odot}$, with a $2 M_{\odot}$ core, are tabulated in Tables 1 and 2.

Each model has 200 mesh points of which a quarter have been selected for these tables. The mesh point number, n , for these points is given in column (1). Columns (2), (3), and (4) give the temperature, pressure, and density, respectively. Column (5) shows the hydrogen composition variable; this is the only composition change we consider; the remainder is assumed to be helium and 2% metals, except that the helium and metals in effect “become” neutrons while compressing on to the core, according to the artifice described in § 2. Column (6) gives the opacity, κ ; column (7) the difference between the radiative (∇_r),

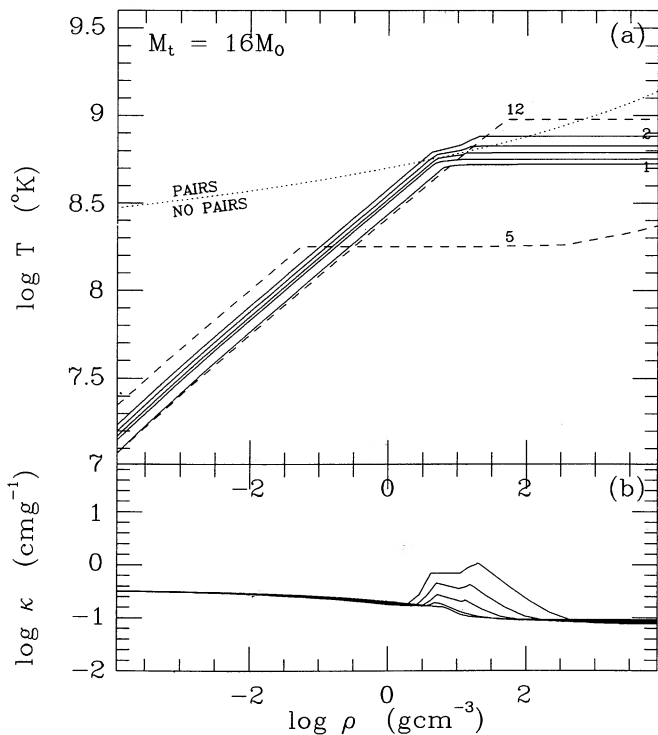


FIG. 6.—(a) Successive temperature-density profiles near the knee for a $16 M_{\odot}$ (type B evolving to type C) model at core masses of 1, 1.4, 1.6, 1.8, and $2 M_{\odot}$ (solid lines). The direction of evolution as the core mass increases is toward higher knee temperatures. Also shown dashed are the 5 and $12 M_{\odot}$ models of TŻ. The line PAIRS/NO PAIRS corresponds to $n_+ = n_e$ in eq. (15) as in TŻ, Fig. 2. (b) The opacity profile for the same models. The opacity increases with core mass.

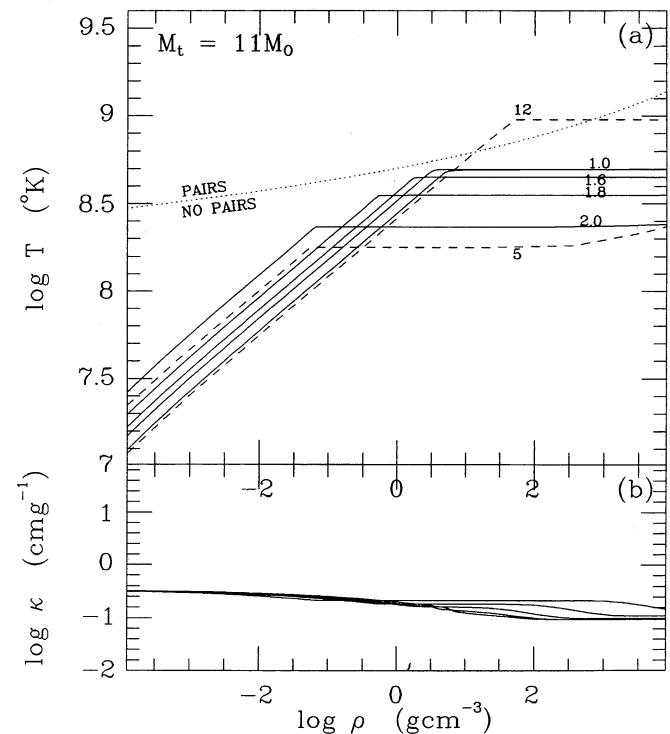


FIG. 7.—As Figs. 6a and 6b but for an $11 M_{\odot}$ model (type B evolving to type A). Evolution is toward lower temperature and density at the knee.

TABLE 1
TYPE A MODEL: TOTAL MASS = 14.45 M_⊙, CORE MASS = 2.0 M_⊙

n^\dagger	T	P	ρ	X^\dagger	κ	$\nabla_r - \nabla_a^\dagger$	v_s	v_{in}	v_c	P_g/P	n_+/n_e	m^\dagger	r	\dot{m}	L	ϵ_q	ϵ_{gr}	ϵ_{nuc}	Δm
	K	dyne	g cm ⁻³		cm g ⁻¹		cm s ⁻¹	cm s ⁻¹				M _⊙	cm	M _⊙ yr ⁻¹	L _⊙	erg g ⁻¹ s ⁻¹	erg g ⁻¹ s ⁻¹		M _⊙
199	8.61	35.66	15.14	0.000	-10.00	-0.189	10.4	...	0.0	0.0	...	0.01	5.20	-8.86	0.90*	1.52	-1.50	...	-1.74
189	8.51	35.05	14.89	0.000	-10.00	-0.288	10.2	...	0.0	0.0	...	1.02	5.87	-8.49	2.38*	1.57	0.51	...	-0.70
179	8.41	33.07	14.01	0.000	-10.00	-0.391	9.6	...	0.0	0.0	...	1.95	6.04	-8.28	2.41*	1.65	2.50	...	-1.78
169	8.41	30.56	12.49	0.000	-10.00	-0.400	9.1	...	0.0	0.0	...	1.99	6.07	-8.29	2.34*	1.51	4.91	...	-4.17
159	8.41	28.04	10.93	0.000	-8.48	-0.403	8.7	...	0.0	0.0	...	2.00	6.07	-8.29	2.24*	1.45	7.55	...	-6.67
149	8.46	25.52	8.99	0.000	-4.36	-0.477	8.4	...	0.0	0.0	...	2.00	6.07	-8.29	2.12*	0.75	9.95	...	-9.19
139	8.59	23.01	6.59	0.000	-1.47	-0.429	8.3	...	0.0	0.0	...	2.00	6.07	-8.29	1.87*	1.36	12.72	...	-11.71
129	8.60	20.56	4.07	0.000	-0.98	-0.294	8.3	...	0.0	-0.1	-9.9	2.00	6.07	-8.29	1.27	1.89	15.55	...	-14.23
125	8.60	19.97	2.99	0.005	-0.98	-0.251	8.6	0.98	0.0	-0.6	-8.4	2.00	6.07	-8.29	2.55	2.84	17.42	17.89	-15.27
123	8.60	19.87	2.23	0.325	-0.86	-0.247	8.9	1.74	0.0	-1.0	-7.2	2.00	6.07	-8.29	3.38	3.27	18.72	18.96	-15.82
121	8.60	19.84	1.53	0.629	-0.77	-0.238	9.2	2.44	0.0	-1.6	-5.9	2.00	6.07	-8.29	3.86	4.30	19.99	18.54	-16.39
120	8.60	19.84	1.23	0.652	-0.76	-0.229	9.4	2.74	0.0	-1.9	-5.4	2.00	6.07	-8.29	4.11	4.59	20.57	18.25	-16.67
119	8.60	19.83	0.93	0.658	-0.76	-0.212	9.5	3.04	0.0	-2.2	-4.8	2.00	6.07	-8.29	4.38	4.87	21.13	17.96	-16.94
118	8.60	19.83	0.64	0.660	-0.76	-0.180	9.7	3.33	0.0	-2.5	-4.2	2.00	6.07	-8.29	4.66	5.15	21.66	17.67	-17.17
117	8.60	19.83	0.34	0.661	-0.76	-0.122	9.8	3.63	0.0	-2.8	-3.6	2.00	6.07	-8.29	4.95	5.42	22.11	17.37	-17.32
116	8.60	19.83	0.06	0.661	-0.76	-0.037	9.9	3.91	0.0	-3.0	-3.0	2.00	6.07	-8.29	5.21	5.29	22.19	17.09	-17.17
115	8.60	19.83	-0.10	0.661	-0.76	-0.004	10.0	4.08	0.0	-3.2	-2.7	2.00	6.07	-8.29	5.29	5.68*	21.61	16.91	-16.95
113	8.60	19.82	-0.16	0.661	-0.76	0.000	10.1	4.13	5.6	-3.3	-2.7	2.00	6.07	-8.29	5.30	6.01*	15.28*	16.82	-16.52
110	8.58	19.75	-0.20	0.662	-0.75	0.004	10.0	4.16	6.0	-3.3	-3.1	2.00	6.08	-8.29	5.30	5.99*	16.15*	16.61	-15.87
105	8.39	18.99	-0.77	0.662	-0.68	0.071	9.9	4.45	6.5	-3.3	-9.6	2.00	6.22	-8.29	5.30	5.80*	17.22*	13.92	-15.18
100	8.08	17.72	-1.71	0.662	-0.58	0.193	9.8	4.84	6.7	-3.2	...	2.00	6.50	-8.29	5.30	5.47*	17.76*	8.85	-15.22
95	7.76	16.45	-2.65	0.662	-0.53	0.290	9.6	5.07	6.9	-3.2	...	2.00	6.85	-8.29	5.30	5.11*	17.81*	4.38	-15.04
90	7.43	15.15	-3.55	0.662	-0.51	0.345	9.4	5.10	6.9	-3.2	...	2.00	7.29	-8.29	5.29	4.66*	17.37*	-1.10	-14.55
85	7.12	13.90	-4.36	0.662	-0.49	0.367	9.2	4.86	6.9	-3.0	...	2.00	7.81	-8.29	5.29	4.08*	16.39*	-5.19	-13.74
80	6.84	12.79	-4.98	0.662	-0.49	0.377	9.0	4.40	6.9	-2.8	...	2.00	8.35	-8.29	5.29	3.48*	15.02*	-7.11	-12.75
75	6.61	11.85	-5.44	0.662	-0.49	0.384	8.7	3.83	6.8	-2.6	...	2.00	8.86	-8.29	5.29	2.95*	13.53*	-8.93	-11.70
70	6.40	11.03	-5.80	0.662	-0.48	0.390	8.5	3.22	6.7	-2.3	...	2.00	9.35	-8.29	5.29	2.46*	12.01*	...	-10.63
65	6.21	10.27	-6.11	0.662	-0.48	0.395	8.3	2.60	6.6	-2.1	...	2.00	9.81	-8.29	5.29	1.99*	10.49*	...	-9.55
60	6.03	9.56	-6.38	0.662	-0.48	0.402	8.0	1.97	6.6	-1.8	...	2.00	10.27	-8.29	5.29	1.54*	8.97*	...	-8.47
55	5.86	8.87	-6.63	0.662	-0.47	0.424	7.8	1.32	6.5	-1.5	...	2.00	10.71	-8.29	5.29	1.09*	7.45*	...	-7.39
50	5.69	8.21	-6.86	0.662	-0.44	0.492	7.6	0.68	6.4	-1.3	...	2.00	11.15	-8.29	5.29	0.66*	5.94*	...	-6.31
45	5.53	7.57	-7.08	0.662	-0.41	0.591	7.4	0.02	6.3	-1.0	...	2.00	11.59	-8.29	5.29	0.23*	4.43*	...	-5.23
40	5.37	6.96	-7.27	0.662	-0.34	0.810	7.2	...	6.3	-0.8	...	2.00	12.01	-8.29	5.29	-0.20*	2.92*	...	-4.15
35	5.20	6.38	-7.46	0.662	-0.23	1.376	7.0	...	6.2	-0.5	...	2.00	12.44	-8.29	5.29	-0.63*	1.41*	...	-3.07
30	5.03	5.83	-7.63	0.662	-0.08	2.827	6.8	...	6.2	-0.3	...	2.02	12.85	-8.33	5.29	-1.10*	-0.18*	...	-1.99
25	4.86	5.35	-7.80	0.662	0.15	7.029	6.7	...	6.1	-0.2	...	2.25	13.27	-9.89	5.29	-1.61*	-3.28*	...	-0.92
21	4.72	4.99	-7.95	0.662	0.45	14.036	6.6	...	6.0	-0.1	...	3.58	13.58	-7.94	5.29	-2.00*	-2.17	...	-0.20
17	4.58	4.58	-8.16	0.662	0.54	12.597	6.4	...	5.9	-0.1	...	7.03	13.80	-8.00	5.29	-2.28*	-2.22	...	0.02
13	4.35	4.14	-8.32	0.662	0.85	51.101	6.3	...	6.0	0.0	...	10.85	13.92	-8.26	5.29	-2.66*	-2.27	...	-0.13
8	4.02	3.49	-8.50	0.662	1.36	99.999	6.0	...	5.6	0.0	...	13.58	13.99	-8.50	5.29	-2.63*	-1.69	...	-0.44
5	3.77	3.13	-8.43	0.662	-1.42	3.842	5.9	...	6.1	0.0	...	14.15	14.00	-8.58	5.29	-4.05*	-1.73	...	-1.43
4	3.67	3.08	-8.38	0.662	-2.39	0.625	5.8	...	5.6	0.0	...	14.20	14.00	-8.58	5.29	-4.05*	-2.56	...	-1.22
3	3.60	3.00	-8.39	0.662	-2.74	0.324	5.8	...	5.5	0.0	...	14.27	14.00	-8.58	5.29	-4.82*	-2.84	...	-1.08
2	3.54	2.86	-8.47	0.662	-3.22	-0.085	5.8	...	0.0	0.0	...	14.36	14.00	-8.59	5.29	-6.00*	-3.36*	...	-1.02
1	3.50	2.68	-8.61	0.662	-3.58	-0.264	5.8	...	0.0	0.0	...	14.45	14.00	-8.60	5.29	-5.75*	-2.72*	...	-1.10

NOTE.—Three dots: log(x) < 0, or log(x) < -10 according to context.

* log(-x) instead of log(x).

† All quantities log₁₀ unless marked †.

TABLE 2
TYPE C MODEL: TOTAL MASS = 14.45 M_{\odot} , CORE MASS = 2.0 M_{\odot}

$n \dagger$	T K	P dyne cm^{-2}	ρ g cm^{-3}	$X \dagger$	κ cm g^{-1}	$\nabla_r - \nabla_a \dagger$	v_s	v_{in} cm s^{-1}	v_c	P_g/P	n_+/n_e	$m \dagger$ M_{\odot}	r cm	\dot{m} $M_{\odot} \text{ yr}^{-1}$	L L_{\odot}	ϵ_g	ϵ_{gr} $\text{erg g}^{-1} \text{ s}^{-1}$	ϵ_{nuc}	Δm M_{\odot}
199	8.64	35.66	15.14	0.000	-10.00	-0.189	10.4	...	0.0	0.0	...	0.01	5.19	-8.55*	1.09*	1.27	-1.17*	...	-1.76
189	8.53	35.08	14.91	0.000	-10.00	-0.284	10.2	...	0.0	0.0	...	0.96	5.86	-8.81*	2.61*	1.37	0.19*	...	-0.72
179	8.44	33.19	14.08	0.000	-10.00	-0.390	9.7	...	0.0	0.0	...	1.95	6.04	-8.53	2.70*	1.61	2.16	...	-1.69
169	8.43	30.75	12.61	0.000	-10.00	-0.400	9.2	...	0.0	0.0	...	2.00	6.07	-8.50	2.68*	1.59	4.54	...	-4.00
159	8.44	28.29	11.09	0.000	-8.74	-0.407	8.7	...	0.0	0.0	...	2.00	6.07	-8.50	2.65*	1.68	7.10	...	-6.44
149	8.53	25.83	9.20	0.000	-4.65	-0.534	8.4	...	0.0	0.0	...	2.00	6.07	-8.50	2.62*	1.10	9.55	...	-8.90
144	8.71	24.60	7.99	0.000	-2.73	-0.514	8.4	...	0.0	0.0	...	2.00	6.07	-8.50	2.60*	1.30	11.05	...	-10.12
139	8.82	23.37	6.73	0.000	-1.33	-0.448	8.4	...	0.0	0.0	-9.8	2.00	6.07	-8.50	2.56*	1.29	12.42	...	-11.35
129	8.85	21.15	4.23	0.000	-1.10	-0.260	8.5	...	0.0	-0.3	-4.7	2.00	6.07	-8.50	2.52*	1.58*	15.56	...	-13.82
128	8.85	21.02	3.96	0.000	-1.10	-0.254	8.6	...	0.0	-0.4	-4.2	2.00	6.07	-8.50	2.16*	1.88*	16.04	...	-14.08
127	8.85	20.94	3.69	0.000	-1.10	-0.251	8.7	0.07	0.0	-0.6	-3.6	2.00	6.07	-8.50	1.42*	2.19*	16.56	...	-14.34
125	8.85	20.85	3.13	0.000	-1.10	-0.249	8.9	0.63	0.0	-1.1	-2.5	2.00	6.07	-8.50	2.79	2.80*	17.65	...	-14.89
123	8.85	20.82	2.56	0.000	-1.07	-0.246	9.2	1.20	0.0	-1.6	-1.4	2.00	6.07	-8.50	3.47	3.24*	18.78	...	-15.45
121	8.85	20.82	1.99	0.000	-0.83	-0.230	9.5	1.77	0.0	-2.2	-0.4	2.00	6.07	-8.50	4.06	3.89*	19.90	...	-16.00
119	8.85	20.81	1.41	0.000	-0.33	-0.092	9.8	2.35	0.0	-2.8	0.4	2.00	6.07	-8.50	4.64	4.52*	20.69	...	-16.21
115	8.84	20.79	1.20	0.000	-0.16	-0.000	9.9	2.56	0.0	-3.0	0.6	2.00	6.07	-8.50	4.70	4.32*	18.49	...	-15.34
112	8.82	20.71	1.08	0.004	-0.24	-0.000	9.9	2.66	0.0	-3.0	0.5	2.00	6.08	-8.50	4.78	4.49*	18.47	...	-14.69
111	8.80	20.63	0.90	0.167	-0.26	0.092	9.9	2.83	6.0	-3.0	0.4	2.00	6.09	-8.50	4.96	5.05	19.54	...	-14.48
110	8.76	20.47	0.57	0.660	-0.33	0.205	10.0	3.11	6.3	-3.0	0.0	2.00	6.11	-8.50	5.18	5.04*	19.38	...	-14.29
105	8.46	19.26	-0.33	0.662	-0.70	0.070	9.9	3.57	6.4	-3.0	-7.6	2.00	6.34	-8.50	5.29	4.75*	15.78*	...	-14.39
100	8.15	18.03	-1.25	0.662	-0.60	0.184	9.7	3.93	6.6	-3.0	...	2.00	6.62	-8.50	5.29	4.44*	16.27*	...	-14.43
95	7.84	16.79	-2.17	0.662	-0.54	0.277	9.5	4.19	6.7	-3.0	...	2.00	6.94	-8.50	5.29	4.13*	16.41*	...	-14.32
90	7.53	15.54	-3.07	0.662	-0.51	0.334	9.4	4.32	6.8	-3.0	...	2.00	7.33	-8.50	5.29	3.82*	16.23*	...	-14.00
85	7.22	14.28	-3.94	0.662	-0.50	0.361	9.2	4.27	6.8	-2.9	...	2.00	7.79	-8.50	5.29	3.47*	15.62*	...	-13.42
80	6.91	13.07	-4.69	0.662	-0.49	0.374	8.9	3.97	6.8	-2.7	...	2.00	8.31	-8.50	5.29	3.05*	14.53*	...	-12.57
75	6.65	12.01	-5.27	0.662	-0.49	0.382	8.7	3.48	6.8	-2.5	...	2.00	8.85	-8.50	5.29	2.59*	13.14*	...	-11.56
70	6.42	11.10	-5.71	0.662	-0.48	0.388	8.5	2.91	6.7	-2.3	...	2.00	9.35	-8.50	5.29	2.12*	11.64*	...	-10.51
65	6.22	10.30	-6.06	0.662	-0.48	0.395	8.2	2.30	6.6	-2.0	...	2.00	9.83	-8.50	5.29	1.67*	10.13*	...	-9.44
60	6.03	9.55	-6.36	0.662	-0.48	0.402	8.0	1.68	6.6	-1.8	...	2.00	10.29	-8.50	5.29	1.22*	8.61*	...	-8.36
55	5.85	8.85	-6.62	0.662	-0.47	0.425	7.8	1.04	6.5	-1.5	...	2.00	10.74	-8.50	5.29	0.78*	7.10*	...	-7.28
50	5.68	8.17	-6.86	0.662	-0.44	0.499	7.6	0.40	6.4	-1.2	...	2.00	11.19	-8.50	5.29	0.35*	5.59*	...	-6.21
45	5.52	7.53	-7.08	0.662	-0.40	0.604	7.4	...	6.3	-1.0	...	2.00	11.62	-8.50	5.29	-0.07*	4.08*	...	-5.13
40	5.35	6.92	-7.28	0.662	-0.33	0.851	7.2	...	6.3	-0.7	...	2.00	12.05	-8.50	5.29	-0.50*	2.57*	...	-4.05
35	5.19	6.33	-7.47	0.662	-0.22	1.466	7.0	...	6.2	-0.5	...	2.00	12.47	-8.50	5.29	-0.93*	1.05*	...	-2.97
30	5.02	5.79	-7.64	0.662	-0.07	3.021	6.8	...	6.2	-0.3	...	2.02	12.89	-8.54	5.29	-1.40*	-0.55*	...	-1.89
25	4.85	5.31	-7.81	0.662	0.18	7.675	6.7	...	6.1	-0.2	...	2.31	13.31	-9.73*	5.29	-1.94*	-3.25	...	-0.82
21	4.71	4.95	-7.97	0.662	0.49	15.037	6.5	...	6.0	-0.1	...	3.90	13.61	-8.19*	5.29	-2.42*	-2.46	...	-0.17
17	4.57	4.55	-8.18	0.662	0.54	12.317	6.4	...	5.9	-0.1	...	7.45	13.81	-8.20*	5.29	-2.92*	-2.40	...	0.01
13	4.33	4.11	-8.33	0.662	0.89	61.685	6.3	...	6.0	0.0	...	11.09	13.92	-8.31*	5.29	-3.40*	-2.29	...	-0.16
8	4.01	3.47	-8.51	0.662	1.35	99.999	6.0	...	5.6	0.0	...	13.63	13.99	-8.41*	5.29	-3.48*	-1.58	...	-0.47
5	3.77	3.13	-8.43	0.662	-1.48	3.467	5.9	...	6.0	0.0	...	14.17	14.00	-8.44*	5.29	-4.62*	-1.63	...	-1.42
4	3.67	3.08	-8.38	0.662	-2.41	0.608	5.8	...	5.6	0.0	...	14.21	14.00	-8.44*	5.29	-4.96*	-2.43	...	-1.22
3	3.60	2.99	-8.40	0.662	-2.75	0.310	5.8	...	5.4	0.0	...	14.28	14.00	-8.44*	5.29	-5.38*	-2.72	...	-1.08
2	3.54	2.86	-8.47	0.662	-3.23	-0.091	5.8	...	0.0	0.0	...	14.37	14.00	-8.45*	5.29	-7.10	-3.18*	...	-1.04
1	3.50	2.68	-8.61	0.662	-3.58	-0.264	5.8	...	0.0	0.0	...	14.45	14.00	-8.45*	5.29	-6.30	-2.57*	...	-1.12

NOTE.—Three dots: $\log(x) < 0$, or $\log(x) < -10$ according to context.

* $\log(-x)$ instead of $\log(x)$.

† All quantities \log_{10} unless marked †.

and adiabatic (∇_{ad}) gradients; and columns (8)–(10), the sound speed v_s , inflow velocity v_{in} , and convective velocity v_c . Column (11) gives the contribution of gas pressure, P_g , to the total pressure P ; and column (12), the ratio of pairs, n_+ , to ionization electrons, n_e . In column (13) is the active gravitational mass, m ; in column (14), the radius variable, r ; and in column (15), the rate of change of m with respect to time at a given mesh point. Since the mesh moves only very slowly in the star, this is almost exactly equal to the mass inflow rate. Column (16) gives the luminosity variable in solar units, and columns (17)–(19) list the contributions to the luminosity from the change in internal energy of the matter at a given mesh point, ϵ_q , the release of gravitational energy from the flow of matter through that mesh point, ϵ_{gr} , and the release of energy from nuclear reactions, ϵ_{nuc} , all in cgs units. The last column, Δm , shows the mass increment between successive mesh points in the full model.

The two models of Tables 1 and 2 have practically the same radius, luminosity, and effective temperature, but for the type A case (Table 1) $L_{\text{nuc}}/L_{\text{grav}} \approx 0.01$, whereas in the type B case (Table 2) $L_{\text{nuc}}/L_{\text{grav}} \approx 5$ with an accretion rate correspondingly 6 times smaller. In the former $T_{\text{knee}} \approx 4 \times 10^8$ K, there are no pairs, and no significant hydrogen burning takes place above the knee. In the latter $T_{\text{knee}} \approx 7 \times 10^8$ K, pairs dominate ionization electrons by a factor of 6 or so, and hydrogen is exhausted by a few meters below the knee. For stars evolving at constant mass, we find a discontinuity at about $13 M_{\odot}$. Below this mass, the temperature and density at the knee decrease, resulting in a type A structure; above it, the knee temperature increases with increasing core mass, leading to a type C structure. We have found no intermediate models in the region of overlap.

Viewed externally, all our models are extreme M supergiants. Such stars with white dwarf cores are known to undergo rapid mass loss, and one would expect similar behavior of a TZO. An empirical relation for red supergiant mass

loss (Kudritzki & Reimers 1978) gives rates of $0.3\text{--}3 \times 10^{-5} M_{\odot} \text{ yr}^{-1}$ for a typical type B/C model. Under these circumstances, the envelope would be lost in $\sim 10^6$ yr, before the core could accrete more than a few hundredths of a solar mass. Such short lifetimes would substantially reduce the number of TZOs expected in the Galaxy and hence the prospects of observing one directly.

As mentioned earlier, the location of our solutions in the M_c - M_t plane differs somewhat from that of TZ. Their calculations were based on a core of $1 M_{\odot}$ and radius 10 km; our equation of state gives a radius nearer 13 km at $1 M_{\odot}$ falling to 10 km only near the OV limit of $2 M_{\odot}$. Though the effects of increasing mass and decreasing radius are not clearly distinguishable, we consider it probable that a softer equation of state for the core would expand region C downward, squeezing out the type B solutions and possibly increasing the area of overlap between cases A and C. More significant may be our use of nuclear reaction rates applicable to the CNO cycle, which allows our type C models to achieve sufficient energy from nuclear burning at knee temperatures $\sim 10^{8.7}$ K. Biehle (1991) in a detailed study of nuclear burning within the framework of the TZ supergiant models finds that knee temperatures must be $\sim 10^9$ K to give the desired luminosity. This would increase the importance of pairs at the knee for a given core mass and have a similar effect to that conjectured for a softer equation of state above.

This work was supported in part by NSF grant PHY89-04035. R. Cannon and P. Eggleton are grateful to the Institute for Theoretical Physics, University of California at Santa Barbara, for their hospitality while part of this work was carried out; to Professor E. P. J. van den Heuvel for organizing a workshop there on "Neutron Stars in Close Binaries;" and to many of the participants at this workshop for their helpful comments.

REFERENCES

- Biehle, G. T. 1991, *ApJ*, 380, 167
 Cooperstein, J. 1988, *Phys. Rev. C*, 37, 786
 Crampton, D., & Hutchings, J. B. 1981, *ApJ*, 251, 604
 Eggleton, P. P. 1971, *MNRAS*, 151, 351
 ———. 1972, *MNRAS*, 156, 361
 Eggleton, P. P., Faulkner, J., & Flannery, B. P. 1973, *A&A*, 23, 325
 Eich, C., Zimmerman, M. E., & Thorne, K. S. 1989, *ApJ*, 346, 277
 Fabian, A. C., Eggleton, P. P., Hut, P., & Pringle, J. E. 1986, *ApJ*, 305, 333
 Flannery, B. P., & van den Heuvel, E. P. J. 1975, *A&A*, 39, 61
 Hulse, R. A., & Taylor, J. H. 1975, *ApJ*, 195, L51
 Joss, P. C., & Rappaport, S. A. 1984, *ARA&A*, 22, 537
 Kudritzki, R. P., & Reimers, D. 1978, *A&A*, 70, 227
 Margon, B. 1984, *ARA&A*, 22, 507
 Miller, G. 1990, *ApJ*, 356, 572
 Oppenheimer, J. R., & Volkoff, G. M. 1939, *Phys. Rev.*, 56, 374
 Phinney, E. S., & Kilkarni, S. R. 1991, *Nature*, in press
 Ruffert, M., & Müller, E. 1990, *A&A*, 238, 116
 Thorne, K. 1977, *ApJ*, 212, 825
 Thorne, K., & Żytkow, A. N. 1975, *ApJ*, 199, L19
 ———. 1977, *ApJ*, 212, 832
 Zimmerman, M. E. 1979, Ph.D. thesis, California Institute of Technology, chap. 6 (available as Caltech Orange-Aid Preprint, 586).